SUPPLEMENTAL MATERIAL

Mechanisms of atrial-selective block of sodium channel by ranolazine II. Insights from a mathematical model

Vladislav V. Nesterenko,[1] Andrew C. Zygmunt,[1] Sridharan Rajamani,[2] Luiz Belardinelli,[2] Charles Antzelevitch [1]

[1]Masonic Medical Research Laboratory, Utica, NY
[2]Gilead Sciences, Palo Alto, CA

Methods

Reduction of the complete sodium channel activation scheme to the 3-states model.

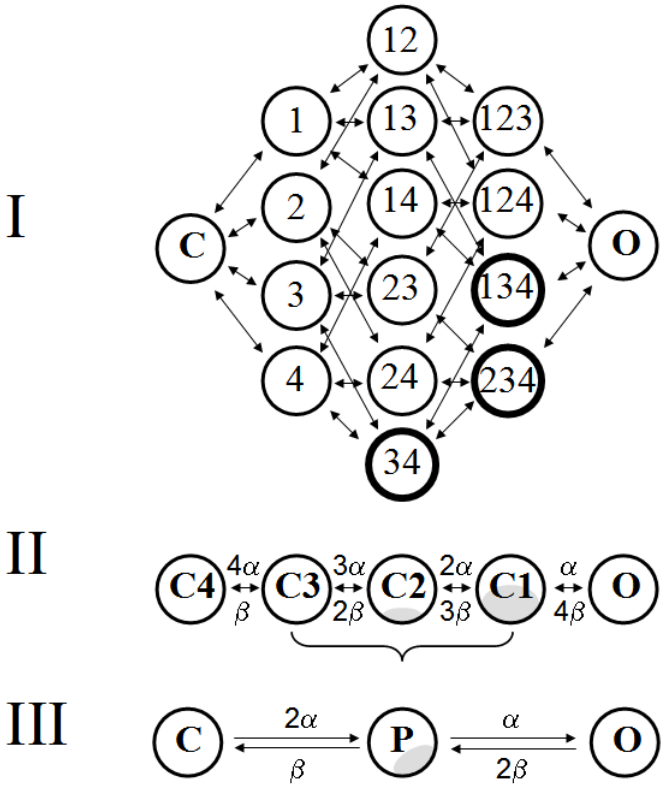

Supplemental Figure 1. Reduction of a complete Markov chain model for sodium channel activation (**I**) to a standard Markov chain model for indistinguishable gates (**II**) to the minimal Markov chain model for activation gating (**III**). Numbers on scheme **I** indicate which activation gate(s) are open in each state. The total number of "pre-open" states in scheme **I** is 14, only 3 states have both activation gates **3** (DIII) and **4** (DIV) in open position (indicated by thick circles). In schemes **II** and **III** the fractions of states C2, C1 and P available for interaction with ranolazine are marked with a gray color to emphasize the fact that only a fraction **δ** of these states should be used when calculating ranolazine binding to the pre-open state P.

The complete model **I** (Supplemental Figure 1) must be used when all four activation gates have different kinetics (3, 4) or when only certain channel states permit interaction with a blocker.(17) However, such schemes require assignment of kinetic rates for drug interaction with all the channel states, which cannot be obtained experimentally. Given these limitations, we reduced the complex multi-state model to a simpler equivalent version. When all gates are identical, the complete scheme **I** can be reduced to the less complex scheme **II**, which is widely used to describe normal and modified sodium channel kinetics.(2, 6) However, neither the distribution of the channels between states C3, C2, and C1, nor the kinetics of drug interaction with each of these states can be obtained experimentally. For this reason we further reduced the activation model by combining three transient closed states (C3, C2, and C1) into a single pre-open state **P**, and introduce a parameter **δ**, which indicates a fraction of the pre-open state **P**, which is able to interact with a blocker (scheme **III**). Such a scheme is mathematically equivalent to the more complex schemes **I** and **II** and can be used for qualitative simulations of drug interaction with the sodium channel. Channel kinetic rates α & β in scheme **III** were adjusted to obtain realistic sodium channel activation parameters and sigmoid (second power) activation time course.

Normal sodium channel gating

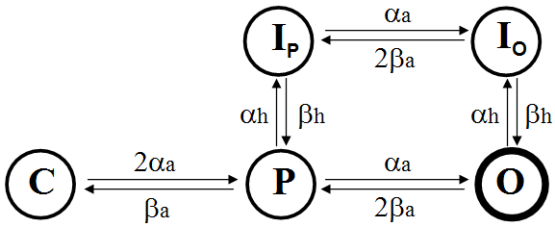

Supplemental Figure 2. The kinetic Markovian model for normal sodium channel gating. State **C** is a fully closed state, state **O** is a fully conducting state, and state **P** represents "pooled" pre-open states

The kinetic Markovian model of sodium channel gating developed in this study contains only five channel states (Figure 2). Here **C** denotes a fully closed state when all activation gates are in closed position. **P** is an aggregate of pre-open states, which combines all states with at least one, but not all activation gate in open position. **O** is an open state when all activation gates are in open position and channel is conducting ionic current. Activation/deactivation transitions **C** ⇔ **P** ⇔ **O** were simplified as if there were only two activation gates. The inactivation process is assumed to be coupled with activation and does not start unless at least one activation gate is open.(5, 17) Thus, the rate of inactivation depends on the fraction of channels in states **P** and **O** at any given potential. In addition, inactivation/recovery rates α_h and β_h have intrinsic voltage dependence. Consequently, this scheme shows inactivated states $\mathbf{I_P}$ and $\mathbf{I_O}$, but the close-inactivated state $\mathbf{I_C}$ is absent. This model is able to reproduce all essential features of normal channel gating, including activation and inactivation time constants and steady-state parameters observed experimentally.

Steady-state activation and activation rate (ms^{-1}) for the fast and slow (late) I_{Na}.

$$a_\infty(V) = \frac{1}{1+\exp\left(-\frac{V-V_a}{4.6}\right)} \quad (1)$$

$$p_\infty(V) = \sqrt{a_\infty(V)} \quad (2)$$

$$\tau_a = \frac{0.25}{\exp\left(-\frac{V-V_a}{20}\right)+\exp\left(\frac{V-V_a}{12}\right)} + 0.0075 \quad (3)$$

$$\alpha_a(V) = \frac{p_\infty(V)}{\tau_a(V)} \quad (4)$$

$$\beta_a(V) = \frac{1-p_\infty(V)}{\tau_a(V)} \quad (5)$$

Rates of activation $\alpha_a(V)$ and deactivation $\beta_a(V)$ were defined via the steady-state activation curve $a_\infty(V)$ and activation time constant $\tau_a(V)$. As is evident from the scheme on

Figure 1, the model assumes a two-step process of activation (C $\Rightarrow$ P $\Rightarrow$ O) as if there were only two gates. This assumption results in voltage dependence for the pooled pre-open state P, i.e. $p_\infty(V)$, to be a square root of the steady-state activation curve $a_\infty(V)$.

Voltage of the half activation at steady-state was set to V_a = −41 mV for the ventricular sodium current and V_a = −47 mV for the atrial sodium current in agreement with our experimental observations.

Steady-state inactivation and inactivation rate (ms^{-1}) for the <u>fast</u> I_{Na} at 15°C.

$$HH(V) = \exp\left(\frac{V - V_h}{6.5}\right) \tag{6}$$

$$h_\infty(V) = \frac{1}{1 + HH(V)} \tag{7}$$

$$\tau_h(V) = \frac{25}{\exp\left(-\frac{V - V_h - 10}{30}\right) + \exp\left(\frac{V - V_h - 10}{12}\right)} + 0.75 \tag{8}$$

$$\alpha_h(V) = \frac{1 - h_\infty(V)}{\tau_h(V)} \tag{9}$$

$$\beta_h(V) = \frac{h_\infty(V)}{\tau_h(V)} \tag{10}$$

Voltage of the half <u>intrinsic</u> inactivation (property of inactivation gates without taking activation into account) voltage was set to V_h = −85 mV for the ventricular sodium current and V_h = −100 mV for the atrial sodium current. Note, that the observable steady-state inactivation curves, as can be obtained using standard experimental protocols, are different from those given by these expressions for intrinsic inactivation, as described below.

The steady-state probability to find a channel in pre-open state P at negative potentials below activation threshold, i.e. the probability that any one activation gate is open, but channel is not yet conducting is given by

$$P_\infty(V) = 2 \cdot p_\infty(V) - a_\infty(V) \tag{11}$$

Using this expression, the voltage-dependence of the <u>observable</u> steady-state inactivation can be calculated as:

$$h_{\infty obs}(V) = \frac{1}{1 + P_\infty(V) \cdot HH(V)} \tag{12}$$

where $P_\infty(V)$ is defined in eq.(11) and HH(V) is defined in eq.(6)

Note, that this observable steady-state inactivation curve depends on channel activation and is shifted significantly to the right (more positive potentials) as compared with the intrinsic steady-state inactivation $h_\infty(V)$.

The model also predicts that the time constant for inactivation and recovery as observed using standard experimental protocols will differ from its intrinsic voltage dependence and can be expressed as:

$$\tau_h(V) = \frac{1}{\alpha_h(V) \cdot P_\infty(V) + \beta_h(V)} \tag{13}$$

This expression is accurate for all voltages below activation threshold between −140 and -60 mV.

Inactivation rate (ms^{-1}) for the <u>slow</u> (late) I_{Na} at 15°C.

In order to simulate inactivation-deficient (slow or late) sodium current we decreased the inactivation rate by the factor of 10 and removed the second exponential term (replaced by 1) to keep the rate practically constant for voltages above −30 mV.

$$\tau_h(V) = \frac{25 \cdot 10}{\exp\left(-\frac{V - V_h - 10}{30}\right) + 1} + 0.75 \qquad (14)$$

With this modification, the simulated time constant for inactivation at −30 mV is ≈200 ms. This value is in agreement with our data, obtained in canine left ventricular myocytes (120-220 ms), and with values, obtained by other investigators (100-500 ms). All other parameters of the sodium channel gating remained the same.

This slowly inactivated state could be incorporated as an additional state in the sodium channel model. However, it would require adding corresponding non-inactivated states and would make the model unnecessarily complex. We chose to simulate the slow sodium current as an independent current with the same activation rate and slow inactivation rate. This approach permits direct comparison of model prediction with experimental data obtained using an inactivation-deficient sodium channel.（25） This model can be applied to simulate ranolazine block of the late component of the fast sodium current under the assumption that channels do not recover from fast inactivation at depolarized potentials.

Inactivation rate (ms^{-1}) for the <u>fast</u> I_{Na} at 37°C in <u>voltage clamp</u> conditions.

Our voltage clamp experiments using canine left ventricular myocytes showed that the inactivation time constant for the fast sodium current at −30 mV is equal to 1.33 ± 0.10 ms at 15°C and to 0.53 ± 0.07 ms at 37°C. The ratio of these time constants is about 2.5, which corresponds to Q_{10} = 1.5 and is within a range previously found for the sodium channel inactivation.（8, 12） Therefore, for voltage-clamp simulations at 37°C we increased the rate of inactivation 2.5 times for all voltages as shown below:

$$\tau_h(V) = 0.4 \cdot \left(\frac{25}{\exp\left(-\frac{V - V_h - 10}{30}\right) + \exp\left(\frac{V - V_h - 10}{12}\right)} + 0.75 \right) \qquad (15)$$

Activation and inactivation rates (ms^{-1}) for the <u>fast</u> sodium current at 37°C in <u>physiological</u> conditions.

Voltage dependences for steady-state activation, steady-state inactivation, and activation time constants were shifted by 20 mV in a positive direction such that V_a = −21 mV for the ventricular sodium current, V_a = −27 mV for the atrial sodium current, intrinsic V_h = −65 mV for the ventricular sodium current and V_h = −80 mV for the atrial sodium current.（7） The rate of inactivation was increased 2.5 fold as in the voltage clamp conditions.

Sodium concentrations and maximal conductance of the sodium current.

Sodium current traces were calculated using simulated open probability O(t) and Goldman-Katz expression for the maximal channel conductance:

$$I_{Na}(t) = \bar{P}_{Na} \cdot O(t) \cdot \left(z_{Na}^{\,2} \times \frac{VF}{RT} \times \frac{\gamma_{Na,i} \cdot [Na]_i \cdot \exp(z_{Na} VF/RT) - \gamma_{Na,o} \cdot [Na]_o}{\exp(z_{Na} VF/RT) - 1} \right) \quad (16)$$

where $[Na]_i$ = 5 mmol/L and $[Na]_o$ = 10 mmol/L for voltage clamp simulations at 15oC and 37°C; and $[Na]_i$ = 10 mmol/L and $[Na]_o$ = 140 mmol/L for AP clamp simulations at 37°C. Activities $\gamma_{Na,i}$ = $\gamma_{Na,o}$ = 0.75. Value of the maximal permeability P_{Na} was adjusted to give realistic amplitudes of the simulated current (in our simulations absolute value of the sodium current does not play any role in ranolazine blockade).

Steady-state activation curves were obtained by dividing the peak of I_{Na} at different voltages by the linear driving force (Vstep − E_{Na}) in agreement with the conventional analysis of experimental data.

Kinetics of ranolazine interaction with the sodium channel

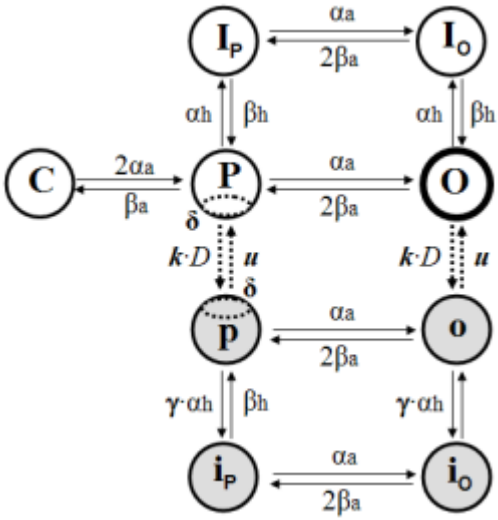

Supplemental Figure 3. Complete scheme of sodium channel gating and block by ranolazine. White circles represent drug-free channel gating and grayed circles represent gating of the blocked channel. Dotted arrows represent ranolazine binding/unbinding and solid arrows represent voltage-dependent channel gating. Parameter δ = 3/14 indicates the fraction of pre-open states P and p that permit ranolazine binding/unbinding. Factor γ = 5.0 represents an increase of the intrinsic inactivation rate of the blocked channels.

The model assumes that ranolazine interaction with its binding site does not depend on the transmembrane potential or channel state. However, binding and unbinding of ranolazine to this site via a hydrophilic pathway are modulated by both activation and inactivation gates. As the scheme in Figure 3 shows, ranolazine access to the binding site is blocked when all four activation gates are closed (no **C** ⇒ **c** transition). Moreover, ranolazine presence in the channel prevents simultaneous closing of all four activation gates (no **p** ⇒ **c** transition) as explained below. These two assumptions eliminate the closed-blocked state **c** and correspondingly the closed-inactivated-blocked state $\mathbf{i_c}$ from the scheme. We also assumed that closing of the inactivation gate completely blocks the hydrophilic pathway to and from the binding site. As a result, ranolazine cannot bind to the inactivated channel so that there is no inactivated-state block. Ranolazine also cannot unbind from the channel when the inactivation gate closes after binding occurs, trapping ranolazine inside the inactivated channel. This leaves the pre-open state **P** and the fully open state **O** as the only states that provide a hydrophilic pathway for ranolazine binding and unbinding. Ranolazine has full access to and from the binding site when the channel is in the open state **O** or the open-blocked state **o**. However, it interacts with the

same kinetic rates only with a fraction δ = 3/14 of the aggregate pre-open states **P** and **p** as detailed below.

Kinetic rates of ranolazine interaction with the binding site of the sodium channel were assumed to be identical for atrial and ventricular sodium channels and were set $k = 3\ \mu M^{-1}s^{-1}$ and $u = 6\ s^{-1}$ in agreement with experimentally calculated values (Table 1, the accompanying paper).

The same kinetic rates were used to simulate ranolazine block of both fast and slow sodium currents based on recent experimental evidence that the same sodium channel protein ($Na_V1.5$) is responsible for both sodium current components in canine and human myocardium.（14，15）

Ranolazine prevents channel from being fully closed

The 3D structure of the ranolazine molecule depends on the particular environment. According to a NIH database（20）there are six different 3D structures that ranolazine can have according to chemical modeling. There is no information about possible ranolazine structure when it interacts with the sodium channel. If we assume that ranolazine acquires the most elongated structure when interacting with the sodium channel, as shown on Figure 1 in the main paper, then its length (22 Å) may span from the local anesthetic (LA) binding site to the site of activation gate interactions. This will hamper normal interaction among activation gates and prevent channel from becoming fully closed (all four gates closed) when ranolazine is bound to the channel. However, it does not prevent any three activation gates from closing. Correspondingly, the closed-blocked state **c** was eliminated from the kinetic scheme (Figure 1A in the main paper).

Ranolazine interaction with pre-open state.

Ranolazine is an open state blocker and requires a hydrophilic pathway to reach the binding site on the main α-subunit. The model assumes that opening of two activation gates DIII and DIV, which contain the LA binding site, is necessary to provide such a pathway. Therefore, only a fraction δ of the aggregate state **P** is accessible for ranolazine. This fraction corresponds to all cases when both gates DIII and DIV are open, but at least one other gate is closed, and is equal to 3/14 for a channel with four activation gates. Correspondingly, ranolazine cannot unbind from the channel when one of these two gates (DIII and DIV) is closed. Therefore, in the kinetic equation for ranolazine interaction with pre-open states **P** and **p**, only the fraction δ of each state is involved in interaction, effectively decreasing kinetic rates:

$$\frac{dP}{dt} = -k_a(\delta \cdot P) + u_a \cdot (\delta \cdot p) = -\delta \cdot k_a \cdot P + \delta \cdot u_a \cdot p \qquad (17)$$

Starmer at al.（23）observed that block acquired in the presence of lidocaine during a train of 20-msec pulses to different potentials below activation threshold follows the same voltage dependence as the probability to find a single activation gate open. Based on this observation they proposed that lidocaine strongly interacts with a transient pre-open state (“non-open state encountered in transitions between a rest potential to a depolarized potential”（23）). However, in the case of lidocaine a slower interaction with the inactivated state of the channel predominates in the overall block development because the sodium channel spends significantly longer time in this state. Subsequently, Sheet & Hanck（18，19）showed that stabilization of voltage sensors of DIII and DIV in the open position effectively increases binding rate of lidocaine block, presumably because activation gates DIII & DIV remain open with a higher probability.

Ranolazine immobilization of activation gates leads to faster intrinsic inactivation

Ranolazine binding to the sodium channel and interference with the normal closing of the activation gates may also increase probability for activation gates to stay in the open position. Since we assumed that inactivation is coupled with activation, the opening of at least one activation gate is required to expose the binding site for the inactivation gate, which is necessary to complete the inactivation process. A higher probability for an activation gate to stay in the open position when ranolazine is bound to the channel increases the probability that the binding site for the inactivation gate will be exposed. This may lead to a faster kinetic rate of the intrinsic inactivation that corresponds to the shift of the voltage-dependence of the intrinsic steady-state inactivation of the blocked channels to more negative potentials. However, this shift of the intrinsic steady-state inactivation of the blocked channels does not affect the observable steady-state availability curve because ranolazine should unbind from the channel before the channel becomes available for opening. Thus, the recovery from the inactivation of the drug-free channels remains unaltered and it is independent from the recovery of blocked channels, which is mainly determined by ranolazine unbinding. We tested possible effects of this mechanism on the overall channel behavior and found that even a 10-fold increase of the inactivation rate of the ranolazine-blocked channel has minimal effect on the position of the observable steady-state availability curve obtained using standard voltage-clamp protocol (results not shown). However, such increase in the inactivation rate of the blocked channels shifts voltage-dependence of ranolazine unbinding to more negative voltages. We found that 5-fold increase of inactivation rate of ranolazine-blocked channels, which is equivalent to 10.5 mV shift of intrinsic availability curve, places the voltage dependence of the tonic block in the voltage range observed experimentally. Thus, the value of the factor γ in the scheme above was set to 5.0.

Expressions describing ranolazine interaction with the sodium channel at sub-threshold potentials according to the scheme on Supplemental Figure 3 (excluding transient binding to the fully open state)

The rate of ranolazine binding as a function of voltage

$$\mathrm{RateF}(V) = \frac{\delta \cdot k_a \cdot P_\infty(V)}{1 + P_\infty(V) \cdot HH(V)} \qquad (18)$$

where δ is a fraction of pre-open state accessible for ranolazine, k_a is the kinetic binding rate for the fully accessible binding site (3 $\mu M^{-1}s^{-1}$), $P_\infty(V)$ is defined in eq.(11) and HH(V) is defined in eq.(6).

The rate of ranolazine unbinding as a function of voltage

$$\mathrm{RateR}(V) = \frac{\delta \cdot u_a}{1 + \gamma \cdot HH(V)} \qquad (19)$$

where u_a is the kinetic unbinding rate for the fully accessible binding site (6 s^{-1}), γ is the factor, which reflects increase of the inactivation rate due to drug binding, and HH(V) is the exponent defined in eq.(6).

Using the rates define above, the effective $K_D(V)$ can be calculated as

$$K_{D,\mathrm{eff}}(V) = \frac{\mathrm{RateR}(V)}{\mathrm{RateF}(V)} = \frac{K_D}{P_\infty(V)} \cdot \frac{1 + P_\infty(V) \cdot HH(V)}{1 + \gamma \cdot HH(V)} \qquad (20)$$

where $K_D = u_a / k_a$ reflects ranolazine binding to the fully accessible binding site (2 μM), $P_\infty(V)$ is the steady-state probability of the pre-open state, defined in eq.(11), and HH(V) is the exponent defined in eq.(6). Note that $K_{D,\mathrm{eff}}$ increases at very negative potentials inversely proportional to the fraction of channels in the pre-open state.

Kinetic rates of interaction of other antiarrhythmic drugs at 15°C.

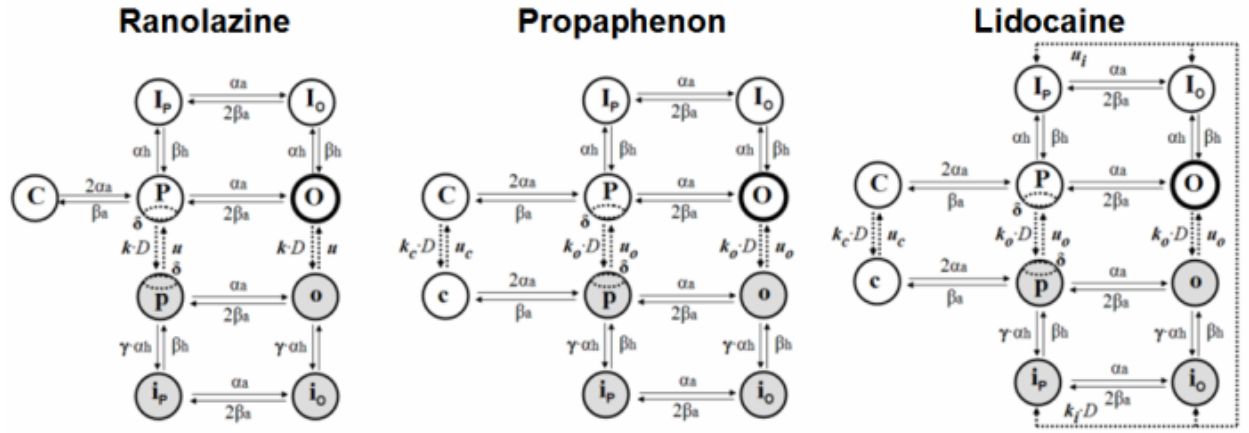

Supplemental Figure 4. Schemes of ranolazine, propafenone, and lidocaine interactions with sodium channels. Kinetic rates are shown in Table 1. The same values of the trapping/guarding coefficient δ = 3/14 and the factor describing effect of a drug on intrinsic inactivation of blocked channels γ = 5 were used for all three antiarrhythmic drugs.

Supplemental Figure 4 shows Markov schemes of drug-channel interactions for three sub-classes of sodium channel blockers. Ranolazine interacts exclusively with pre-open/open states, is trapped in inactivated state, and prevents activation gates from closing at negative potentials. Propafenone predominantly interacts with pre-open/open states, is trapped by inactivation gate, and trapped by closed activation gates at negative voltages, interacting with the closed state with a very low rate. For illustrative purposes we disregarded possible interaction of propafenone with inactivated state of the sodium channel as described by Edrich et al.(9) Lidocaine interacts with all channel states and corresponding kinetic rates of interaction decrease in the following order: pre-open/open − inactivated − closed.

Supplemental Table 1. Kinetic rates of antiarrhythmic drug interaction with different states of the sodium channel that were used to simulate block development (15°C)

Channel state	Kinetic rates & K_D	Ranolazine	Propafenone	Lidocaine
Open	k_o ($\mu M^{-1}sec^{-1}$)	3.0	25.0	1.4
	u_o (sec^{-1})	6.0	12.0	40.0
	K_D (μM)	2.0	0.48	28.5
Closed	k_c ($\mu M^{-1}sec^{-1}$)	–	0.001	0.0007
	u_c (sec^{-1})	–	0.090	1.0
	K_D (μM)	–	90.0	1500.0
Inactivated	k_i ($\mu M^{-1}sec^{-1}$)	–	–	0.036
	u_i (sec^{-1})	–	–	0.67
	K_D (μM)	–	–	18.6

Kinetic rates for ranolazine interaction with the sodium channel were obtained in this study. Kinetic rates for lidocaine and propafenone were adopted from other publications.（9, 21, 23） Corresponding values for kinetic rates at 37°C were obtained using Q_{10} = 1.65 for both kinetic binding and unbinding rate that leaves K_D values unaffected by temperature.

Kinetic rates of interaction of antiarrhythmic drugs at 37°C.

Our experimental study (see Figure 5 C & D in the main paper) of the development of the sodium channel block during pulse trains at 37°C did not permit direct calculations of kinetic rate constants at body temperature due to extremely fast block rate ($\lambda \approx 1.5$ or smaller). Such fast block rate makes exponential fits unreliable and very sensitive to the peak current at the 2nd pulse. Lowering ranolazine concentration can be used to decrease the rate of block development. However, low concentration results in a smaller steady-state block that hampers reliability of the exponential fit. Instead, an appropriate Q_{10} for ranolazine interaction with the sodium channel was found by using a non-linear procedure to minimize the error of fit to the experimentally obtained data. We constrained the fit by choosing the same Q_{10} for both kinetic binding and unbinding rates. This constraint is in agreement with data obtained by Makielski et al.（13） for the temperature dependence of lidocaine interaction with the sodium channel. We found that the best fit can be obtained using Q_{10} = 1.65, which corresponds to approximately 3-fold increase in both kinetic rates between 15°C and 37°C. This value of Q_{10} is somewhat higher than Q_{10}=1.3 for diffusion （11）, but smaller than Q_{10} = 2.6 that can be calculated from the lidocaine data.（13）

Time-course of pre-open/open states and inactivated state simulated using action potential clamp in atrial and ventricular cells.

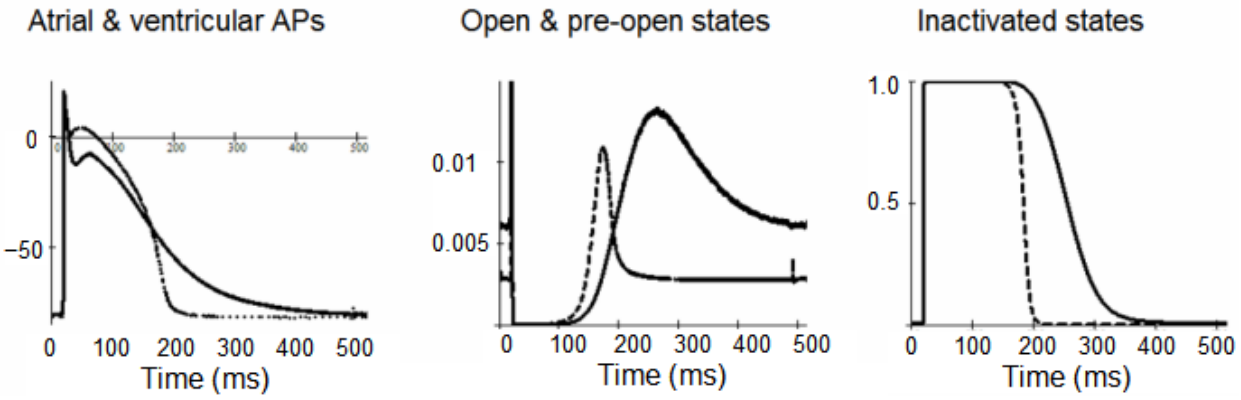

Supplemental Figure 5. **Left** panel: Shapes of ventricular (dashed line) and atrial (solid line) action potentials used in AP-clamp simulations. The time course of pre-open/open states (**middle** panel) and inactivated state (**right** panel) of ventricular and atrial sodium channels when corresponding shape of AP was used as a command potential. During the upstroke of the action potential, a large fraction of channels promptly opens and then inactivate following the path $C \Rightarrow P \Rightarrow O \Rightarrow I_O$. The open probability O reaches the peak ≈ 0.6 − 0.8, and open channels inactivate within 2 ms, as indicated by initial spike in the middle panel, which is outside the vertical range. During repolarization, channels slowly recover from inactivation via $I_P \Rightarrow P$ pathway, which is reflected in the second slow peak in the middle panel.

Implementation of Markovian sodium channel model

Model equations were solved using a 2nd order Runge-Kutta algorithm in MathCad2001 environment running on a personal computer equipped with Intel Xeon CPU 3.00 GHz with 2 Gb of RAM.

Supplementary Data

Normal sodium channel gating.

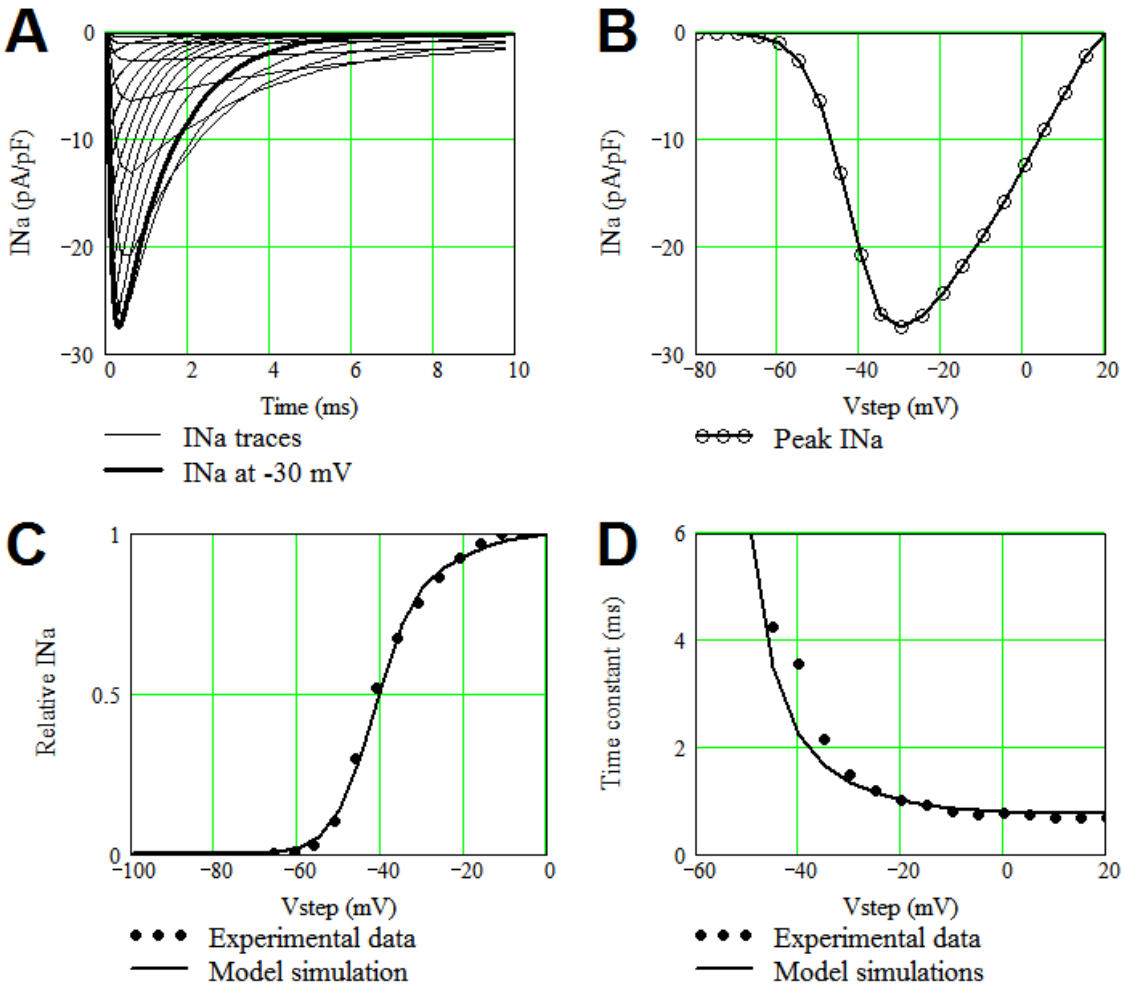

Supplemental Figure 6. Properties of the **ventricular** sodium channel model at 15°C. **Panel A**: current traces simulated for steps to potentials between -80 and +20 mV from holding potential = −140 mV. Thick trace corresponds to the step to −30 mV. **Panel B**: I-V relations for the peak I_{Na} obtained during this voltage protocol. **Panel C**: steady-state activation curve obtained from I-V curve divided by linear driving force $V\text{-}E_{Na}$ (solid line) compared with experimentally determined steady-state activation in the same conditions (circles). **Panel D**: Voltage-dependence of the inactivation time constant obtained using mono-exponential fits to the simulated current traces above (solid line) as compared with experimentally obtained inactivation time constant (circles). Model data (solid lines in C and D) are in good agreement with experimental data (circles).

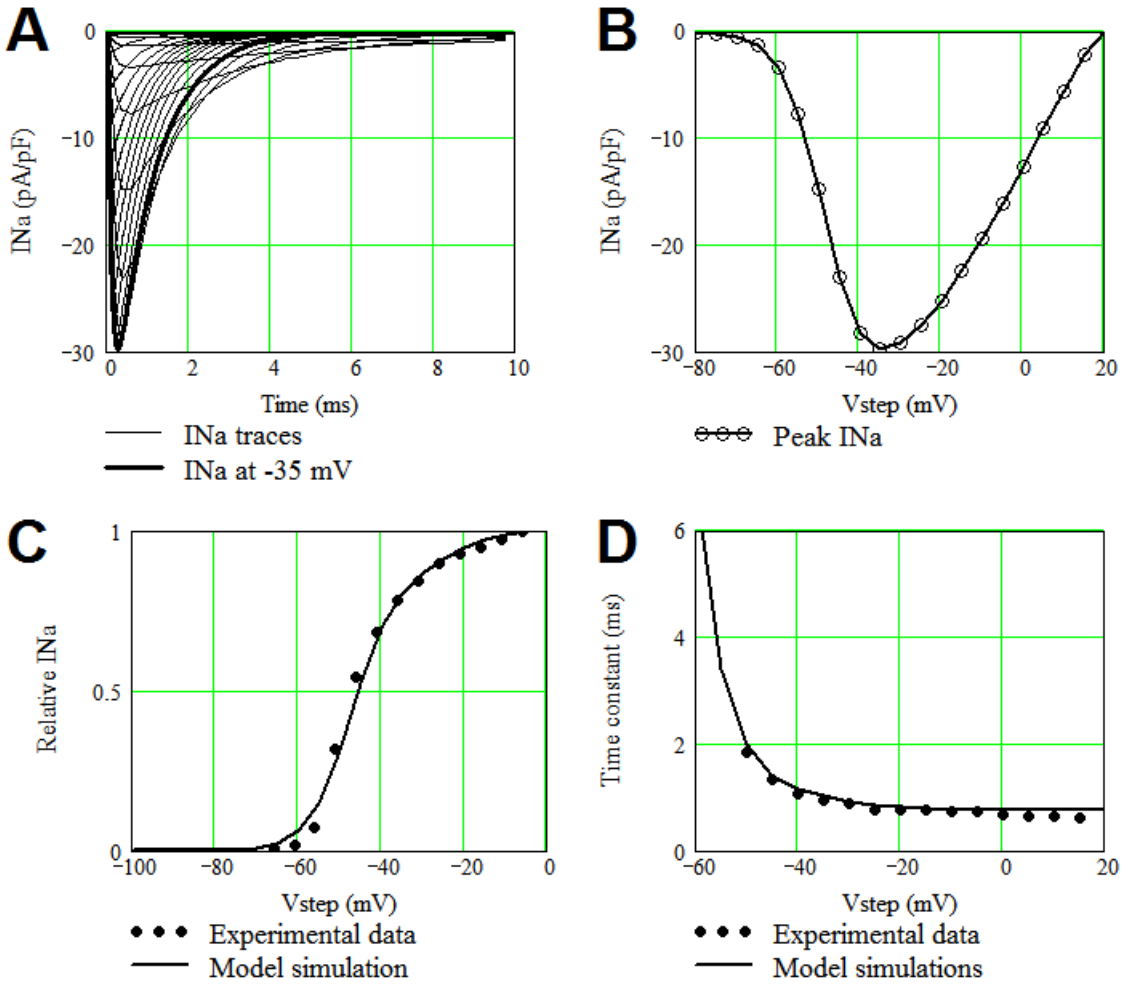

Supplemental Figure 7. Properties of the atrial sodium channel model at 15°C. See Supplemental Figure 6 for panel description. Note that in atrial cells sodium current inactivates faster than in ventricular cells (0.92 msec vs. 1.36 msec at −30 mV) and the steady-state activation is shifted by 5 mV to more negative potentials. The maximum of the I-V curve is also shifted by the same amount. Model data (solid lines in C and D) are in good agreement with experimental data (circles).

Behavior of the simulated fast sodium current was tested against common experimental protocols. For simulations, we used the voltage-clamp protocol identical to that used in experimental studies. Voltage steps were delivered from holding potential of −140 mV to potentials between −80 mV and +20 mV in 5 mV increments. Duration of voltage step was 300 msec with 100 msec between steps. Concentrations of Na^+ ions in extracellular solution (10 mM) and inside the cell (5 mM) were chosen to reflect experimental conditions. With these concentrations reversal potential was E_{Na} = 18.1 mV. Figures 6A and 7A show simulated I_{Na} traces in ventricular (6A) and atrial (7A) myocytes. Figures 6B and 7B shows current-voltage relations for the simulated peak I_{Na} for the two cell types. Comparison of simulated (solid lines) and experimental (circles) steady-state activations for two tissue types are shown on Figures 6C (ventricular cell) and Figure 7C (atrial cell). Fit of Boltzman function to simulated ventricular data yields $V_{½}$ = −39.9 mV and slope = 6.0 mV, while Boltzman fit to experimental data yields $V_{½}$ = −40.13 mV and slope = 6.3 mV. Same analysis of atrial data yields $V_{½}$ = −44.7 mV and slope = 6.6 mV for simulated data and $V_{½}$ = −45.2 mV and slope = 6.5 mV for experimental data. Note

that in order to make analysis of simulated data identical to the analysis of experimental data we calculated the steady-state activation by dividing the peak INa by ($V - E_{Na}$) for both simulated and experimental data even while I_{Na} was simulated using Goldman-Kats expression for the maximal conductance (see Methods). Figures 6D and 7D compare simulated and experimentally observed inactivation time constants. Note good agreement of simulated values and experimental data.

Intrinsic and observable steady-state availability curves for inactivation coupled with activation. Steady-state open and pre-open states ("window").

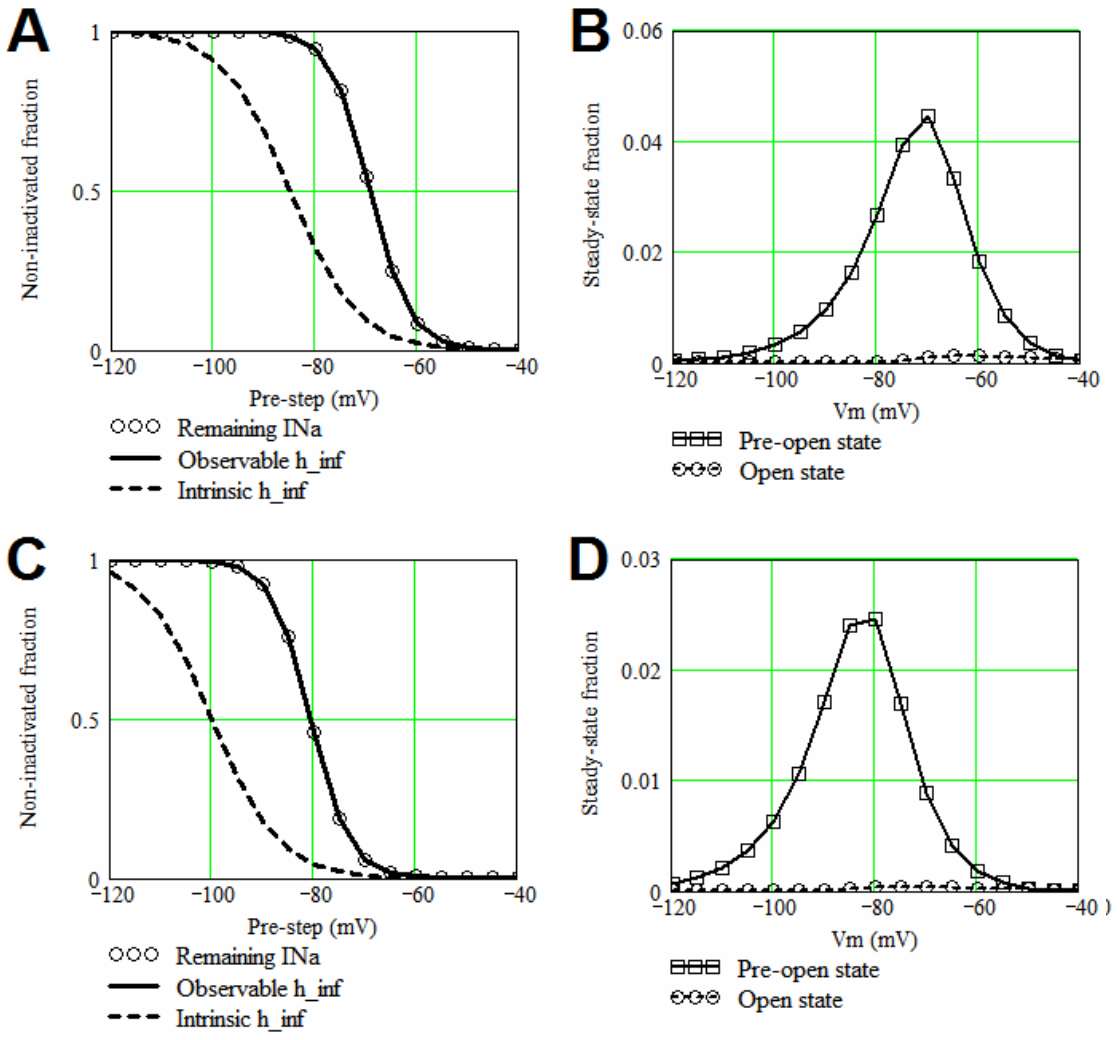

Supplemental Figure 8. Panels A and B illustrate simulated behavior of the ventricular sodium current model. Panels C and D − atrial sodium channel model. **Panels A and C**: Circles depict simulated steady-state inactivation obtained using the standard inactivation protocol and calculated as the decrease of the peak sodium current recorded at −30 mV after 1000 ms prepulse to the indicated potentials. Solid lines were obtained using the theoretical "observable" steady-state inactivation (equation 12). Dashed lines indicate the intrinsic voltage dependence of the steady-state inactivation (equation 7) that were set in the models to have Vh = −85 mV for ventricular and Vh = −100 mV for atrial model. Observable curves are characterized by Vh = −69.3 mV, slope = −3.9 mV (ventricular model) and by Vh = −80.6 mV, slope = −3.8 mV (atrial model). The difference of 11 mV between half-inactivation points in ventricular and atrial models are in the typical range (10-13 mV) observed experimentally in these cell types. **Panels B and D**:

Steady-state probabilities of the pre-open state (squares) and open state (circles) as a function of potential in ventricular (B) and atrial (D) cells. These values were obtained at the end of 1000-msec test steps to corresponding potentials. Steady-state open probability results in non-inactivating window current that peaks at −62.0 mV in ventricular cells and at −74.4 mV in atrial cells. However, maximal open probability in this window of potentials is very small (0.13% in ventricular cells and 0.04% in atrial cells). On the other hand, the peak of the window pre-open probability is 30−60 times larger (4.6% in ventricular cells and 2.6% in atrial cells). Note that the magnitude of the steady-state pre-open probability determines the rate of ranolazine binding to the sodium channel, not the amount of block. As a result of these differences, unbinding of ranolazine from the sodium channel at moderately depolarized potentials below activation threshold is slower in atrial cells, leading to larger accumulation of block between voltage steps or action potentials.

Development of the sodium channel inactivation in control and development of block in the presence of 15 μM ranolazine during the standard inactivation protocol.

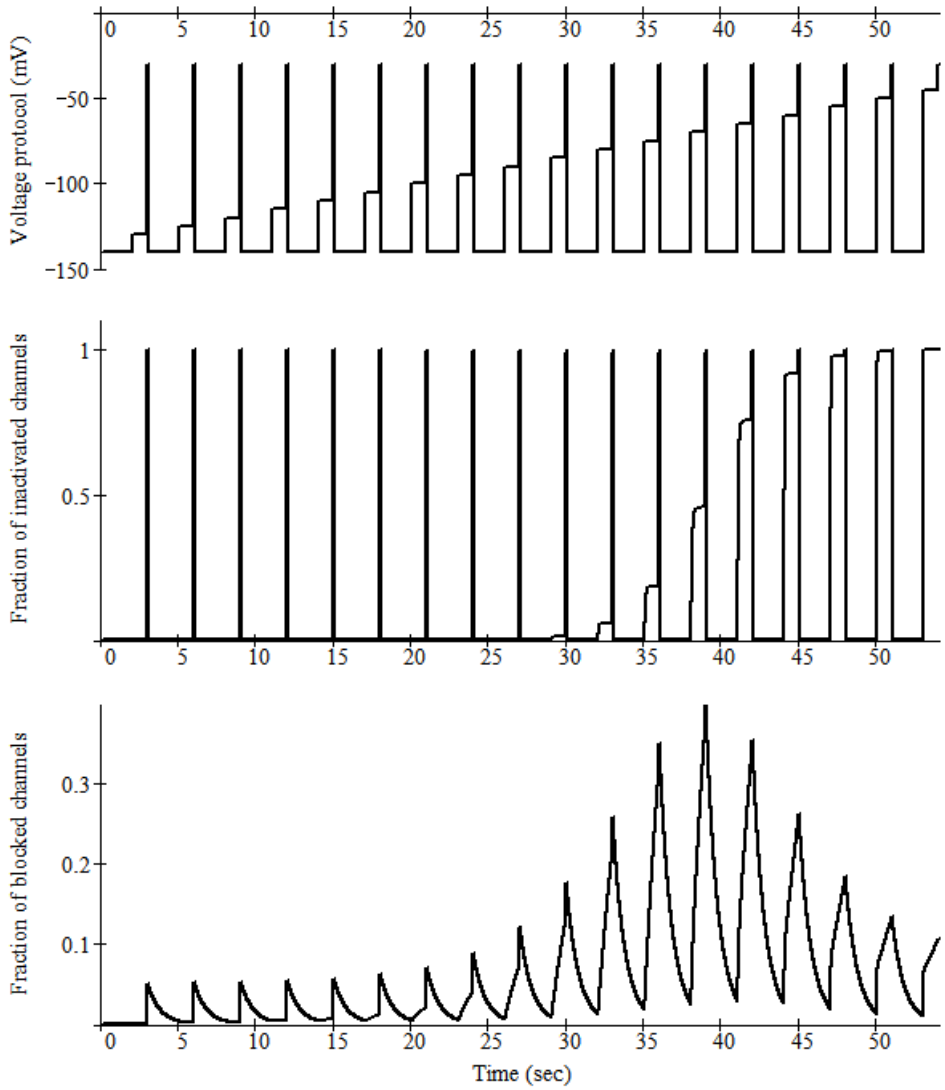

Supplemental Figure 9. Standard steady-state inactivation protocol used to obtain the steady-state availability curve. Cell potential was set to −140 mV for 2 seconds followed by a conditioning pulse for 950 msec and the test pulse to −30 mV for 50 msec. Conditioning steps were delivered between −130 mV and −45 mV with 5 mV increments. Complete voltage protocol is shown on the upper panel. Middle

panel shows time-dependent changes of the fraction of inactivated channels in the absence of ranolazine. Note that 950 msec conditioning step is long enough to attain steady-state inactivation at all voltages. Bottom panel shows the time-dependent changes of the fraction of blocked channels during the same voltage-clamp protocol in the presence of 15 μM ranolazine. The block is far from the equilibrium, especially at more positive voltages.

Supplemental Figure 9 illustrates that standard protocol routinely used to obtain the steady-state inactivation curve is well suited for that purpose in our model. Conditioning pulse ~1000 msec duration to any voltage is long enough for the inactivation process to attain a steady-state value. However, in the presence of ranolazine the fraction of blocked channels is far from its steady-state value for most except very negative potentials. As a result, channel availability curve obtained using this protocol does not reflect equilibrium conditions. It is commonly assumed (a misconception) that 2-3 seconds is enough for any drug to equilibrate with the channel binding site. In case of ranolazine, this time is enough to reach the steady-state block at negative potentials, but the block is far from the steady-state at more positive potentials. This is the cause of a shallower slope of the stead-state availability curve (shifted in the presence of ranolazine). Similar effect is typically reported for other antiarrhythmic drugs.

Effect of pre-pulse duration on the shift of the steady-state availability curve.

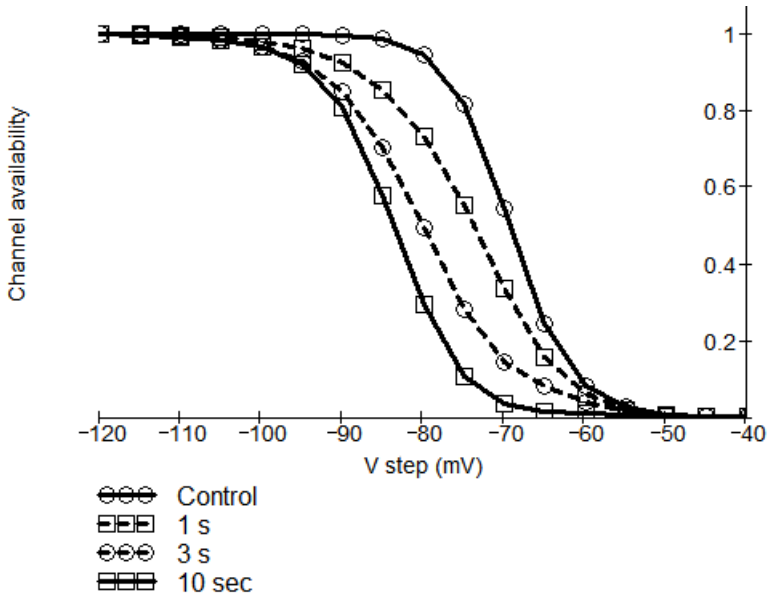

Supplemental Figure 10. Effect of prepulse duration on the position and slope of the steady-state availability curve in the presence of 15 μM ranolazine. Ventricular model only for illustrative purposes. Curve labels are shown below the plot.

The steady-state channel availability curves on Supplemental Figure 10 were obtained using the same voltage protocol, as shown on Supplemental Figure 9 (top panel). Curves were obtained in control conditions and in the presence of 15 μM ranolazine. Standard protocol, which is widely used in these types of experiments, has pre-step duration of 1 s. The simulated channel availability curve is shifted to more negative voltages and becomes less steep. The shift becomes larger when pre-step duration is increased to 2 s. However, the true equilibrium binding at all pre-step potentials can be achieved only for the pre-pulse duration of 10 s or

longer. Note, that the steady-state availability curve obtained using 10 s pre-steps has the same slope as the control curve.

Shift of the steady-state availability curve in the presence of ranolazine.

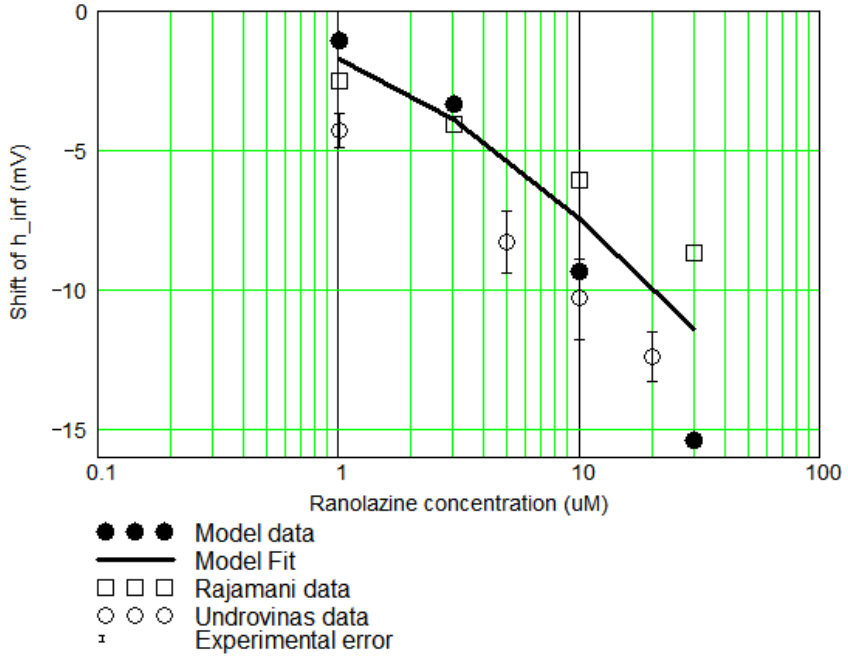

Supplemental Figure 11. This figure illustrates the shift of the steady-state availability curve obtained experimentally by Undrovinas et al.（24）(open circles with error bars) and by Rajamani (unpublished, open squares) in the presence of 10 μM ranolazine. Corresponding model predictions are shown as filled circles. The solid line represent the best fit to the simulated data using Bean's equation.（1）

Previous studies suggested that ranolazine is an inactivated state blocker without providing proper experimental evidence. The only published evidence for the inactivated state block by ranolazine is the shift of the steady-state availability curves in the presence of ranolazine. Bean's equation used for the shift analysis was developed specifically to describe lidocaine (an inactivated state blocker) effect on the steady-state availability curve. It employs only two channel states (closed and inactivated) and excludes any transient state (both pre-open and open). This shift, predicted by the Bean's equation（1）sometimes is erroneously interpreted as a true change in channel gating, while the authors themselves indicated that the observed shift of the availability curve is due to channel's block by lidocaine. Such a block makes an additional fraction of the channels unavailable upon subsequent step to test potential. We have previously described the mechanism of the parallel shift of the steady-state availability curve by inactivated state blockers.

The best fit using Bean's equation to the model simulated data yields K_{Dr} > 1 mM and K_{Da} = 1.8 μM. Corresponding fit to Rajamani et al data gives K_{Dr} = 9.4 μM and K_{Da} = 1.8 μM. Fit to Undrovinas et al data results in K_{Dr} = 7.4 μM and K_{Da} = 1.2 μM. Note that both simulations and Rajamani experiments were obtained for the fast sodium current, while Undrovinas et al. did not observe any shift of the steady-state availability curve using the fast sodium current and reported the shift for the late sodium current. Our data indicate that ranolazine shifts the steady-state availability curve obtained for the fast sodium current. Thus, there is a discrepancy between experimental data, which cannot be accounted in our model.

Our experimental data directly probed ranolazine interaction with the inactivated state. We tested effect of the duration of time that channel spends in the inactivated state on the block. Results indicate that the duration of the voltage step to −30 mV where channels spend most of the time in inactivated state (after transient opening) has no effect on the block. Our model showed that the block of the sodium channels by ranolazine via interaction with pre-open/open states affects the channel availability curve by shifting it to more negative potentials and decreasing the slope.（22）

Thus, our choice of the model (interaction with pre-open state instead of inactivated state) was not based on our arbitrary model selection, but was dictated by experimental observations.

Indirect evidence in favor of ranolazine interaction with pre-open/open state(s) as opposed to inactivated state can be deduced from the well-established fact that ranolazine preferentially blocks the late (slow) INa and accelerates the current decay. It is commonly assumed that the late sodium current is a result of impaired inactivation when channels briefly close to some other state (not the traditional inactivated state), while closing into the inactivated state halts the bursting behavior (i.e. inactivated state is “absorbing”). An inactivated state blocker blocks channel after it is inactivated. However, these inactivated channels already have no contribution to the late current. Therefore, their block would not affect the time-course of the current trace, so that the sensitivity of the fast and late current to an inactivated state blocker will be similar.

Influence of the slow sodium channel inactivation on apparent K_D.

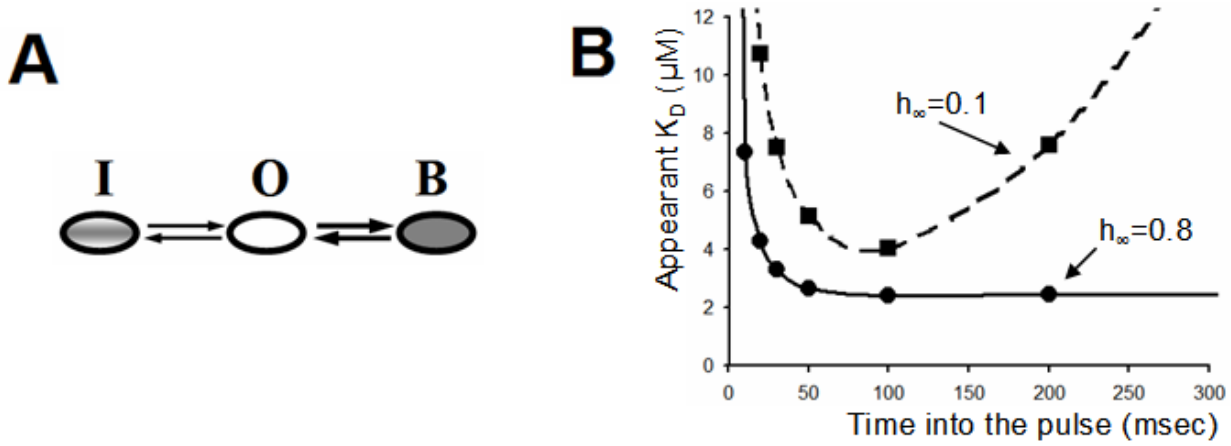

Supplemental Figure 12. Panel A shows a *minimal* scheme illustrating the competition between inactivation and block when rates of both processes have comparable magnitude. Dependence of apparent K_D on the time into the trace, obtained using the minimal scheme is shown in **panel B**. Block was calculated as a relative current decrease compared with control current at different times into current trace. Solid line with circles illustrates apparent K_D for ranolazine block of current inactivating with τ = 50 ms and large non-inactivating component of 80%. Apparent K_D at 50 msec into the trace is 2.4 μM. Dashed line illustrates results simulated for current inactivating with τ = 100 ms and much smaller non-inactivated component of 10%. Apparent K_D at 200 msec into the trace is 7.6 μM.

Figure 12A shows the model scheme of competition between channel inactivation and ranolazine binding, which assumes that the rates of inactivation and drug binding are comparable so that inactivation cannot be considered as being at instant equilibrium. This assumption is probably valid for the slow or late sodium current, which inactivates with the time constant on the order of hundreds milliseconds. In this case, block develops during

depolarization and the amount of block depends on the time into the depolarizing step, when block is assessed. Interaction of ranolazine with the resting slow/late channels will be the same as is observed for the fast sodium channels, because the same channels are responsible for both fast and late sodium current. Figure 12B shows that the apparent K_D for drug block varies as a function of time into the trace because slowly inactivating channels spend most of the time during the pulse to positive potentials in the open state, which is fully available for the ranolazine binding. Obviously, when the dose-response curve is obtained for the peak inward current, block has very little time to develop and a very large concentration of ranolazine is necessary to substantially decrease this peak. As two curves in Figure 12B show, the dependence of the apparent K_D on the time into the trace is influenced by other parameters that characterize the inactivation process. When the maximal steady-state non-inactivating current is large (τ_h = 50 ms; h_∞ = 0.8), the apparent K_D attains a constant value of 2.5 μM, which is equal to the true K_D of 2 μM divided by h_∞. When the current does not inactivate (h_∞ = 1.0), the apparent K_D becomes the true K_D. Conversely, when the current shows substantial inactivation with time (τ_h = 100 ms; h_∞ = 0.1), the apparent K_D attains some minimal value well above the true K_D then increases again at longer times. This effect is due to recovery of blocked channels, so that they transiently become conducting (open) before final inactivation. In a sense, blocked channels "feed" the open state late into the pulse when both inactivation and the blocking processes are almost complete. Note that when the block of the slow current with these characteristics is measured at 200 ms the predicted apparent $K_D \approx 7.6$ μM is in agreement with K_D obtained experimentally in canine ventricular myocytes (Zygmunt, unpublished data, 2009 and (24)). This effect is further enhanced when inactivated state is absorbing and channels do not recover from inactivation at all (h_∞ = 0.0). In these conditions, all channels eventually end up in the inactivated state and no channels will remain in the blocked state. Theoretical analysis of the competition between inactivation and block can be found elsewhere.(10)

Effect of holding potential on the tonic block and on the rate and the steady-state use-dependent block by ranolazine.

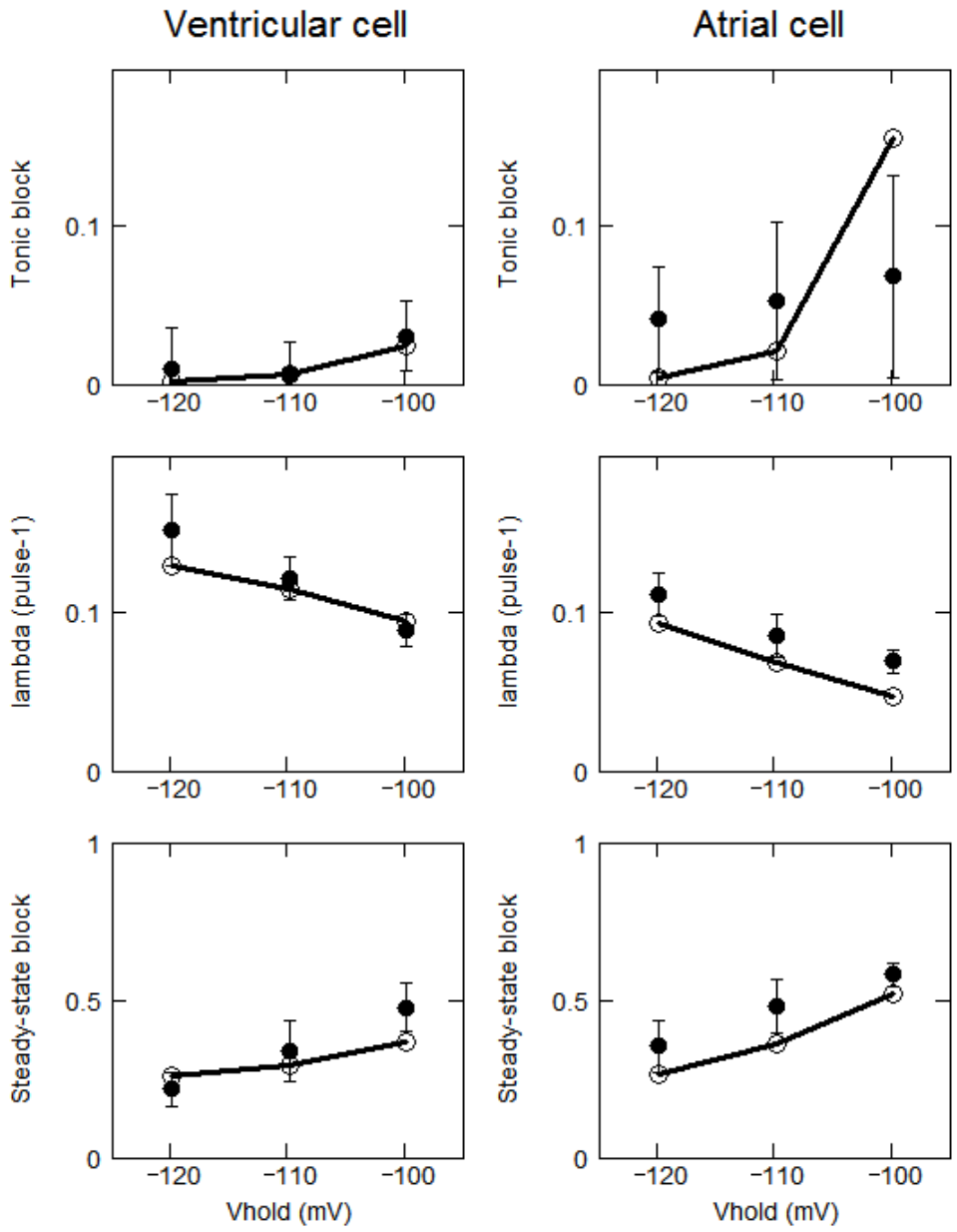

Supplemental Figure 13. Effect of holding potential (−120, −110, and −100 mV) on parameters of block by 10 μM ranolazine at 15°C in the two cell types. Comparisons of simulations (solid lines with open circles) and experimental data (solid circles with S.D. bars). **Panel A** shows tonic block in ventricular (left) and atrial (right) cells obtained during 50-msec pulse to −30 mV after 10 sec rest at corresponding holding potentials as compared with control current. **Panel B** shows the rate of block development (λ in pulses^{-1}) during the same pulse train protocols in ventricular (left) and atrial (right) cells. **Panel C** shows steady-state block attained when the same pulses were repeated 40 times with diastolic interval of 100 msec. Results of simulations are in good agreement with experimental data.

Supplemental Figure 13 illustrate good agreement between the tonic block, the rate of block development, and the steady-state block obtained experimentally during voltage-clamp

pulse trains at 15°C at different holding potentials and corresponding values simulated by the model. Note that these sets of experimental data were not used to calculate kinetic rate constants for ranolazine interaction with the sodium channel. Such a comparison serves as an independent verification of the accuracy of calculated kinetic rates of ranolazine interaction with the sodium channel and the overall accuracy of our model.

Effect of the action potential waveform on the sodium channel block development.

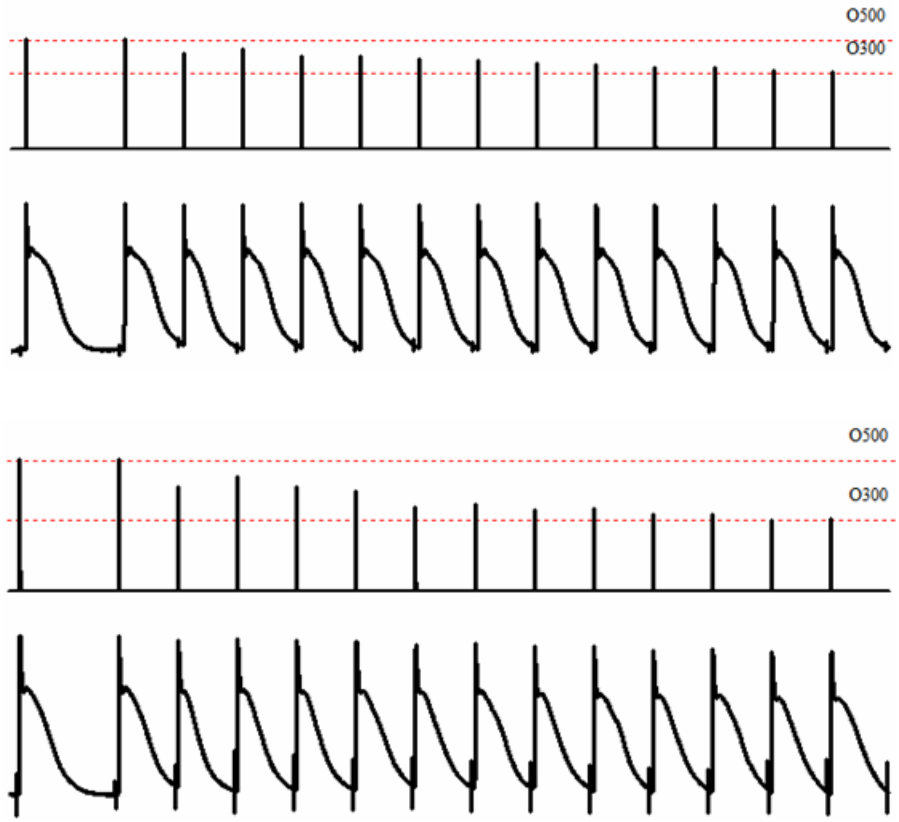

Supplemental Figure 14. These simulations were performed using AP trains recorded experimentally when BCL was shortened from 500 ms (first 2 APs) to 300 ms. A: AP train recorded in control. B: AP train recorded in the presence of 10 μM ranolazine (shown on Fig.6C in the main manuscript). Using the train of APs recorded in control, the model predicts the Vmax ratio (300 ms/500 ms) of 69.7% (30.3% additional block). When the train of APs recorded in the presence of 10 μM ranolazine had been used, this ratio was 54.5% (45.5% additional block). Thus, the prolongation of the terminal phase of the atrial action potential increases the amount of block by 50%.

Block development during the time course of an action potential.

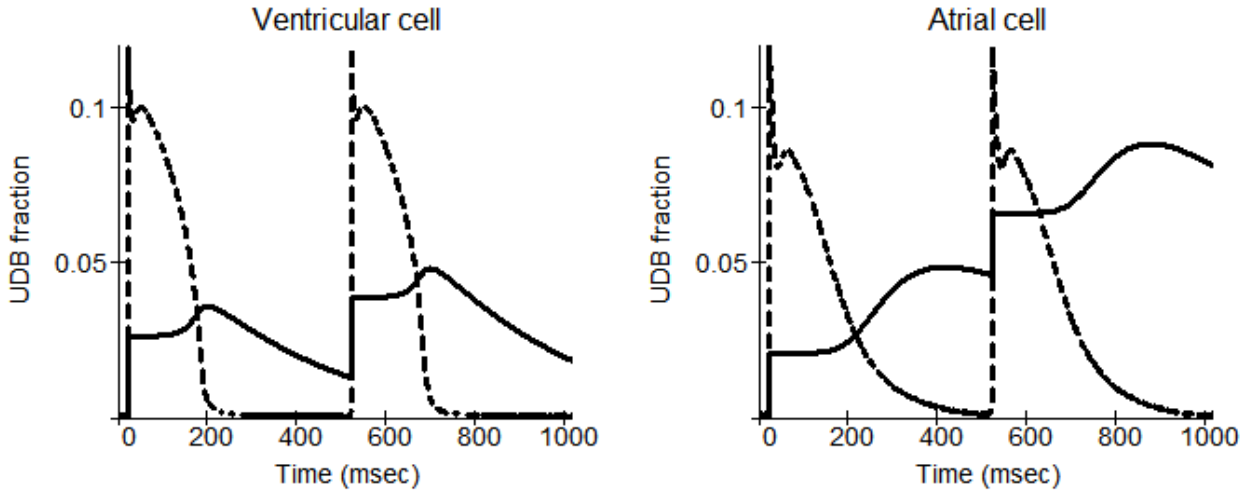

Supplemental Figure 15. Development of the sodium channel blockade during the train of the applied action potential using ventricular (left) and atrial (right) sodium channel model in the presence of 10 μM ranolazine. Dashed lines show action potential clamp waveforms used for these simulations. These traces illustrate block development during the initial two applied APs (shown on Figure 8C in the main text) at expanded time scale.

This Figure shows that the sodium channel block accumulation during an action potential in the presence of ranolazine has two distinct components: (1) a very fast block due to ranolazine binding to the fully open channels during AP upstroke, and (2) a relatively slow block during phase 3 of the action potential due to ranolazine binding to the channels in the pre-open state, i.e. to the channels that have already recovered from inactivation, but not all activation gates are closed yet. The rate of block depends on the fraction of channels in accessible state. The fraction of open channels during upstroke is very large. However, channels spend only a few milliseconds in this state before inactivation. This limits the total block accumulation during AP upstroke to a fraction of the equilibrium block. On the other hand, only a small fraction of channels, which recover from inactivation during repolarization, do not promptly enter the fully closed state. However, channels spend in this state much longer time ranging from tens to hundreds milliseconds. The slow repolarization rate of the atrial action potential provides much longer time for ranolazine to interact with the sodium channels recovering from inactivation into pre-open state.

The choice of the experimental data used for comparison with the model predictions

Wang et al (25) data

Wang at al (25) used three different sodium channel isoforms, including cardiac rNav1.5-WCW. They showed that ranolazine interaction with the sodium channel is similar for all these isoforms. Unfortunately, the authors did not present traces of the slow rNav1.5-WCW block by ranolazine, probably, because they unexpectedly found that ranolazine at low concentrations increases the slow rNav1.5-WCW current recorded at 50 ms into the trace. The authors provided no explanation for this observation, which may reflect competition between inactivation and ranolazine binding (see Supplementary Figure 12 above) or may be an experimental

artifact. For this reason we used traces obtained using inactivation-deficient rNav1.4-WCW (Fig.6 in (25)) for comparison with model simulations.

Rajamani et al (16) data

Slow INa: Figure 1 in (16) shows current traces recorded in HEK293 cells expressing WT and a "non-inactivating" R1623Q mutant sodium channel. However, the R1623Q mutant displays a considerable inactivation. A double exponential fit to the trace presented on their Figure 1 shows two time constants: 3.01 ms and 11.37 ms with relative amplitudes 86% and 11%. The same double exponential fit to a control trace on their Figure 2B gives similar time constants: 3.46 ms and 9.83 ms with the relative amplitudes 71% and 25%. This behavior can hardly be described as "non-inactivating INa." In our model, we used the inactivation time constant for the slow INa close to 200 ms, which is within the range of the late INa inactivation time constants obtained in our laboratory and other studies. The small amplitude of the sodium current at 50 ms into the trace (their Figure 3) makes it very difficult to reliably measure the amount of slow INa block by ranolazine. For these reasons, we found it impossible to compare these experimental results with the model predictions for slow sodium current block by ranolazine.

Peak INa: The main result of Rajamani et al paper (16) − the concentration dependence of fast and late INa block by ranolazine at different pulse frequencies − is presented on Figures 2 in (16). These results show that slow INa is more sensitive to ranolazine than peak INa. Our model reproduces this difference in sensitivity. According to the model prediction (see the main manuscript), the apparent K_D for the slow INa block by ranolazine is 5.2 μM, which is close to IC_{50} values obtained by Rajamani et al (7.45 μM) and by Undrovinas et al (6.46 μM). However, our model cannot reproduce results shown in their Figure 3 − the time course of the block development during pulse trains. There is a large linear component of the use-dependent block development, which fails to reach the steady-state after 40 pulses. We observed similar behavior in our experiments using HEK293 cells expressing WT α- and β-subunits (see Figure 1D in our accompanying experimental paper). However, when we adjusted Na concentrations to record outward INa at the same step potential (Figure 1C in our accompanying paper), the block development followed an exponential time course, as observed in all studies using cardiac myocytes independent of a blocker. Similarly, Wang et al (25) used the outward INa to characterize use-dependent block of several sodium channel isoforms expressed in HEK293 cell and found exponential block development without any linear component (see their Figures 3 and 4). Note that the use-dependent block development should always have a mono-exponential course for all possible binding schemes. This stems from the fact that during each pulse the same fraction of block of the drug-free channels is attained due to repetition of the same voltage pattern during train of pulses (voltage clamp steps or action potentials.) This process is a first order reaction and it is described by the mono-exponential function. We attributed the difference in the block development for inward and outward currents to the Na ion accumulation in the former case due to a relatively small size of HEK293 cells. Correspondingly, our model cannot reproduce results shown on their Figure 2, which were obtained from the measurements as shown on their Figure 3.

Shift of the steady-state availability curve for peak INa

Rajamani et al (16) found that the steady-state availability curve is shifted in the presence of 10 μM ranolazine by 11.5 mV (their Figure 4 and Table 2). On the other hand, Undrovinas et al.(24) found no shift of the steady-state availability curve for peak INa in the presence of 20 μM ranolazine. Thus, the model predictions of the shift of the steady-state

availability curve by 3 mV (atrial cells) or 5 mV (ventricular cells) in the presence of 15 μM ranolazine falls between these experimental values and is in agreement with our experimental findings (see Figure 2 and corresponding discussion in the main paper).

Undrovinas et al (24) data:

Dissociation constants: Using block of the late INa in myocytes from the failing canine heart Undrovinas et al (24) showed that ranolazine blocks late sodium channel at negative potentials (resting state block) with K_{Dr} = 7.42 μM and at positive step potentials (presumably, inactivated state block) with K_{Di} = 1.17 μM. On the other hand, these authors (14, 15) showed that the same sodium channels are responsible for both fast and late sodium currents. Therefore, 10 μM of ranolazine will produce a very substantial block of the sodium channel independent of the channel state. The well established fact that ranolazine at 10 μM has very little effect on the fast sodium current is difficult to reconcile without questioning the validity of the method used to calculate above K_D's.

As we already discussed above (see Supplemental Figure 11 and corresponding text) Undrovinas et al.(24) employed Bean's equation (1) to calculate K_D's, However, this equation is valid only when the channel is in the equilibrium state at a given potential and there are no transient states. Thus, it is not applicable when a drug has strong interaction with the transient state(s) of the channel, such as pre-open or open states, which promptly disappear in equilibrium conditions. Our experimental data (see accompanying experimental paper) provide direct evidence that ranolazine does not interact with the equilibrium state of the sodium channel, which dominates at positive potentials (the inactivated state). Based on this experimental evidence, we excluded ranolazine interaction with the inactivated state of the sodium channel from our numerical model. Results of our simulations indicate that all experimental data, including the shift of the steady-state availability curve, can be explained by ranolazine interaction with pre-open and open states of the sodium channel (Supplementary Figure 11).

Late INa: Our simulations showed similar high sensitivity of the slow sodium current to ranolazine as was obtained by Undrovinas et al. The numerical discrepancy between K_D values can be explained by the interaction between inactivation and block as illustrated on Supplemental Figure 13. In addition we found that the time constants of the late sodium current inactivation both in control and under ranolazine provided on their Figure 5A do not correspond to the values that we obtained by the double exponential fits to the experimental curves shown on the same Figure. We found slow time constants to be 960 ms and 630 ms.

We modified our slow sodium current description to mimic the inactivation rate constant reported by Undrovinas et al (470 ms in control conditions). Supplemental Figure 16 compares experimental data presented in (24) with the model simulation.

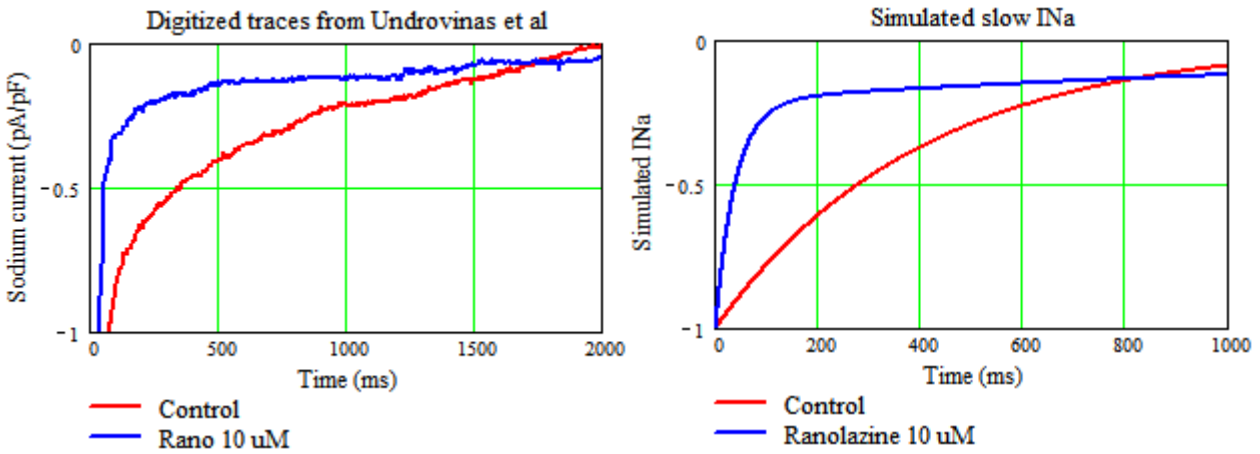

Supplemental Figure 16. Traces re-digitized from the Figure 5A in (24) (**left**) and the model simulations assuming the inactivation time constant of 470 ms in control (**right**). The slow sodium current trace simulated in the presence of ranolazine is better fitted with the double exponential function. Vertical scale for the digitized traces from (24) was decreased from 2 pA/pF to 1 pA/pF in order to emphasize the late current decay. Note the crossover of the two simulated current traces, which is similar to experimental finding. This effect is due to the fast block of open channels at the beginning of the trace that followed by a continuous recovery of non-inactivated blocked channels, which are subsequently inactivated (later in the trace, not visible).

Supplemental Reference List

1. **Bean BP, Cohen CJ, Tsien RW**. Lidocaine block of cardiac sodium channels. *J Gen Physiol* 81: 613-642, 1983.
2. **Bennett PB, Valenzuela C, Chen LQ, Kallen RG**. On the molecular nature of the lidocaine receptor of cardiac Na+ channels. Modification of block by alterations in the alpha-subunit III-IV interdomain. *Circ Res* 77: 584-592, 1995.
3. **Cha A, Ruben PC, George AL, Jr., Fujimoto E, Bezanilla F**. Voltage sensors in domains III and IV, but not I and II, are immobilized by Na^+ channel fast inactivation. *Neuron* 22: 73-87, 1999.
4. **Chanda B, Bezanilla F**. Tracking voltage-dependent conformational changes in skeletal muscle sodium channel during activation. *J Gen Physiol* 120: 629-645, 2002.
5. **Clancy CE, Rudy Y**. Linking a genetic defect to its cellular phenotype in a cardiac arrhythmia. *Nature* 400: 566-569, 1999.
6. **Clancy CE, Zhu ZI, Rudy Y**. Pharmacogenetics and anti-arrhythmic drug therapy: a theoretical investigation. *Am J Physiol Heart Circ Physiol* 292: H66-H75, 2007.
7. **Colatsky TJ**. Voltage clamp measurements of sodium channel properties in rabbit cardiac Purkinje fibres. *J Physiol* 305: 215-234, 1980.
8. **Dumaine R, Towbin JA, Brugada P, Vatta M, Nesterenko DV, Nesterenko VV, Brugada J, Brugada R, Antzelevitch C**. Ionic mechanisms responsible for the electrocardiographic phenotype of the Brugada syndrome are temperature dependent. *Circ Res* 85: 803-809, 1999.
9. **Edrich T, Wang SY, Wang GK**. State-dependent block of human cardiac hNav1.5 sodium channels by propafenone. *J Membr Biol* 207: 35-43, 2005.
10. **Gilliam FR, Starmer CF, Grant AO**. Blockade of rabbit atrial sodium channels by lidocaine. Characterization of continuous and frequency-dependent blocking. *Circ Res* 65: 723-739, 1989.
11. **Hille B**. *Ionic channels of excitable membranes*. Sunderland, MA: Sinauer Associates Inc, 1984.
12. **Kohlhardt M**. Different temperature sensitivity of cardiac Na+ channels in cell-attached and cell-free conditions. *Am J Physiol* 259: C599-C604, 1990.
13. **Makielski JC, Falleroni MJ**. Temperature dependence of sodium current block by lidocaine in cardiac Purkinje cells. *Am J Physiol* 260: H681-H689, 1991.
14. **Maltsev VA, Kyle JJ, Mishra S, Undrovinas AA**. Molecular identity of the late sodium current in adult dog cardiomyocytes identified by $Na_v1.5$-antisense inhibition. *Am J Physiol Heart Circ Physiol* H667-H676, 2008.
15. **Maltsev VA, Kyle JW, Undrovinas A**. Late Na^+ current produced by human cardiac Na^+ channel isoform $Na_v1.5$ is modulated by its b_1 subunit. *J Physiol Sci* 59: 217-225, 2009.
16. **Rajamani S, El-Bizri N, Shryock JC, Makielski JC, Belardinelli L**. Use-dependent block of cardiac late Na^+ current by ranolazine. *Heart Rhythm* 6: 1625-1631, 2009.
17. **Sheets MF, Hanck DA**. Voltage-dependent open-state inactivation of cardiac sodium channels: gating current studies with Anthopleurin-A toxin. *J Gen Physiol* 106: 617-640, 1995.

18. **Sheets MF, Hanck DA**. Molecular action of lidocaine on the voltage sensors of sodium channels. *J Gen Physiol* 121: 163-175, 2003.

19. **Sheets MF, Hanck DA**. Outward stabilization of the S4 segments in domains III and IV enhances lidocaine block of sodium channels. *J Physiol* 582: 317-334, 2007.

20. **Specialized Information Services USNLoM**. ChemIDplus. NIH. http://chem.sis.nlm.nih.gov/chemidplus [21 Dec. 2010].

21. **Starmer CF, Grant AO**. Phasic ion channel blockade: a kinetic model and parameter estimation procedure. *Mol Pharmacol* 28: 348-356, 1985.

22. **Starmer CF, Nesterenko VV, Gilliam FR, Grant AO**. Use of ionic currents to identify and estimate parameters in models of channel blockade. *Am J Physiol* 259: H626-H634, 1990.

23. **Starmer CF, Nesterenko VV, Undrovinas AI, Grant AO, Rosenshtraukh LV**. Lidocaine blockade of continuously and transiently accessible sites in cardiac sodium channels. *J Mol Cell Cardiol* 23 (Suppl.I): 73-83, 1991.

24. **Undrovinas AI, Belardinelli L, Undrovinas NA, Sabbah HN**. Ranolazine improves abnormal repolarization and contraction in left ventricular myocytes of dogs with heart failure by inhibiting late sodium current. *J Cardiovasc Electrophysiol* 17: S161-S177, 2006.

25. **Wang GK, Calderon J, Wang SY**. State- and use-dependent block of muscle $Na_v1.4$ and neuronal $Na_v1.7$ voltage-gated Na+ channel isoforms by ranolazine. *Mol Pharmacol* 73: 940-948, 2008.